

A formal exact mathematical solution for a sloping rat-hole in a highly frictional granular solid

BY G. M. COX, J. M. HILL AND N. THAMWATTANA

*School of Mathematics and Applied Statistics, University of Wollongong,
Wollongong, NSW, 2522, Australia*

This paper provides a formal exact analytical solution to a rat-hole with a sloping base in two and three dimensions for a highly frictional granular material. A rat-hole is the general term used to describe those stable cavities, which frequently occur in storage hoppers and stock piles, whose formation prevents further material falling through the outlet. Figure 1(a) depicts the typical geometric configuration, comprising upper and lower sloping surfaces that form a channel or cylindrical cavity. In granular industries this is a commonly occurring situation, for example, where the flow of material from a hopper ceases due to the formation of a stable almost cylindrical vertical cavity. Despite their practical importance, the only analytical solution applies to the perfectly cylindrical cavity, assumed infinite in length with no upper sloping surface. In order to determine analytical solutions to more realistic situations, it is necessary to make compromises with regard to both geometric and constitutive considerations. Here, for both two and three-dimensional rat-holes, we present analytical parametric solutions for the special case of a highly frictional granular material, where the angle of internal friction is equal to ninety degrees. In addition, we assume that the highly frictional granular material is at the point of yield on a sloping rigid base, and with an infinitesimal central outlet as shown in Figure 1(b). The solutions given here are bona fide exact solutions of the governing equations for a Coulomb-Mohr granular solid, and satisfy exactly the free surface conditions on the sloping upper surface and a frictional condition along the sloping rigid base. We emphasize that while all zero stress boundary conditions are correctly satisfied, and the solutions constitute the only known exact analytical solutions for a

realistic rat-hole geometry, the solutions for both geometries exhibit infinite values of the other stress component on the free surface. This feature arises as a consequence of assuming an angle of internal friction equal to ninety degrees, and throws doubt on the physical applicability of the formal exact solution.

Keywords: highly frictional granular materials; rat-holes;
Coulomb-Mohr yield condition; analytical parametric solutions

1 Introduction

The term rat-hole is used to describe stable two-dimensional slots or channels, or three-dimensional cylindrical cavities, which form in storage hoppers and stock piles and prevent further material falling, under gravity alone, through the outlet. Despite their widespread occurrence in those industries dealing with the storage of granular solids, very little theoretical information is available, and indeed the only mathematical solutions pertaining to the stress analysis of such structures are based upon the classical solution of Jenike (see, for example, Jenike [1, 2]) for a perfectly vertical cylindrical cavity. Further, the precise material conditions are not known for which the phenomena occurs, nor is it known whether a given formed rat-hole is stable or unstable. These and other important issues have yet to be properly addressed in the literature. In this paper we present an analytical solution for both two and three-dimensional rat-holes, where we assume the material has flowed through a central outlet, until the point is reached when there is no further flow of material, as depicted in Figure 1(b). We further suppose that the remaining granular material is in limiting equilibrium, that is static but on the point of yield.

The solutions presented are exact analytical solutions of the equilibrium equations, the Coulomb-Mohr yield condition, and are based upon a number of simplifying assumptions. Firstly, they apply only to the limiting idealized theory for highly frictional granular solids, namely for the special case of an angle of internal friction equal to ninety degrees. While this assumption is made primarily to enable an ana-

Granular material	Measured values of ϕ_e			Calculated values of β		
Coal	69.9	73.3	76.7	0.939	0.958	0.973
Alumina cake	70.2			0.941		
Waste rock	76.9			0.974		
Silica	78.2			0.979		

Table 1: Experimentally measured values of the effective angle of internal friction ϕ_e for certain granular materials, where β is calculated from $\beta = \sin \phi_e$.

lytical solution to be derived, it is also found in laboratory testing that occasionally some materials do indeed give rise to large values of the effective angle of internal friction around 75 degrees, as indicated by the data in Table 1. Further, we assume the rat-hole has a sloping upper surface of infinite extent, containing an infinitesimal central outlet as indicated in Figure 1(b), and that the material obeys a frictional condition along a sloping rigid base, where the material throughout the rat-hole is at the point of yield. We note that rat-holes with a sloping base occur in storage hoppers, while rat-holes with a flat base occur in stock piles. We emphasize again that while all zero stress boundary conditions are correctly satisfied, the solutions presented for both geometries display infinite values of the other stress component on the free surface, indicating possible physical inapplicability, a consequence no doubt of the highly frictional assumption. In particular, the stress components σ_{xx} and σ_{rr} are found to be infinite on the stress free surface for the two and three-dimensional solutions respectively.

The classical rat-hole theory, enunciated by Jenike [1, 2] and Jenike and Yen [3, 4], attempts to address the question of rat-hole stability without recourse to a theory involving velocity components. Practising engineers are sceptical of classical rat-hole theory because it appears not to reflect actual material behaviour. A comprehensive account of existing developments of the theory for flow of materials from silos and hoppers is provided by Roberts [5]. The classification of the two principal modes for flow was introduced by Jenike [1, 2] termed funnel-flow and mass-flow, and these are

shown schematically in Figure 2. Mass-flow has been examined in detail by Jenike [6, 7, 8] and Johanson [9], and the appearance of funnel-flow indicates the occurrence of an unstable rat-hole. Here we are primarily concerned with determining the stress profile within an existing defined rat-hole. In Hill and Cox [10] the classical rat-hole theory is re-examined with a view to determining the validity of the underlying assumptions that lead to the so-called “Jenike stable rat-hole equation”, and some of the assumptions are shown to be invalid. While the classical theory assumes that a rat-hole is a perfectly vertical cylindrical cavity, where the stresses within the rat-hole are independent of height, in reality rat-holes tend to exhibit some variation with height. Such rat-holes are examined in Hill and Cox [11], where some analytical expressions for the stress profile are provided for slightly tapered cylindrical cavities. Spencer and Bradley [12, 13] have given approximate stress and velocity solutions for the related problem of gravity flow within tapering channels and tubes, while Hill and Cox [14] have extended existing rat-hole theory to include granular materials that satisfy the more general shear-index yield condition.

For steady flow from a hopper, Jenike [2, 7, 8] and Johanson [9] examine radial flow solutions for which the equilibrium equations and the Coulomb-Mohr yield condition reduce to give two highly nonlinear coupled ordinary differential equations for the determination of the stress field, which in general can only be solved numerically. However, in the context of a two-dimensional converging wedge shaped hopper, an exact parametric solution of these equations is given by Hill and Cox [15] for the special case of $\beta = 1$, where $\beta = \sin \phi$ and ϕ is the angle of internal friction. This solution is the first exact solution of the highly nonlinear coupled ordinary differential equations that involves two arbitrary constants, and was latter exploited by the same authors in Hill and Cox [16, 17] to determine an exact solution for a two-dimensional wedge shaped stock pile. Further, Cox and Hill [18] derive exact parametric solutions for three-dimensional cone shaped hoppers and stock piles for the special case of $\beta = 1$. We comment that all the special solutions applying for $\beta = 1$ are meaningful mathematical solutions of the governing equations, and as

such, provide limiting bounds for solutions of physically more meaningful materials and benchmarks for numerical schemes.

We note that the special case of $\beta = 1$ corresponds to an angle of internal friction equal to ninety degrees. While such materials may initially be thought to be non-physical, there are granular materials which do indeed exhibit very large angles of internal friction such as those shown in Table 1, and as such, the case $\beta = 1$ is physically plausible as a limiting ideal material. We comment that the data given in Table 1 refers to the effective angle of internal friction ϕ_e , which is generally between zero and ten degrees higher than the angle of internal friction ϕ , noting that for a cohesionless material, the effective angle of internal friction ϕ_e coincides with the angle of internal friction ϕ . Further, the major issue here is not the actual magnitude of the angle of internal friction, but rather the proximity of the sine of the angle in relation to unity, noting that even a value of 64 degrees gives a value close to one, namely $\sin 64^\circ = 0.9$. However, upon examining the published data for the effective angle of internal friction (see, for example, Australian Standard [19] and Perkins [20, 21]), we find that while there exists materials possessing relatively high values of the effective angle of internal friction, for example from the Australian Standard [19] (page 23) we see black and brown coal exhibiting effective angles of internal friction in the ranges of $40^\circ \leq \phi_e \leq 60^\circ$ and $45^\circ \leq \phi_e \leq 65^\circ$ respectively. Although there does not seem to exist any published data for materials possessing effective angles of internal friction comparable to the high values reported in Table 1, Sture [22] reports effective angles of internal friction as high as 70° from tests conducted in a microgravity environment.

Despite this, the analysis presented in this paper may be independently justified due to the fact that the governing equations can be expressed in the form given by (13) and (30), for two and three-dimensional rat-holes respectively. As such, it is evident that approximate perturbation solutions involving powers of $1 - \sin \phi$, as given by (14) and (31) respectively, are plausible. Such perturbation schemes would yield approximate analytical solutions for materials possessing angles of internal

friction ϕ such that $1 - \sin \phi$ approaches zero. It is also clear from (13) and (30), that the exact parametric solutions presented here are precisely the leading term of the respective perturbation schemes.

Here, we exploit the mathematical solutions corresponding to $\phi = \pi/2$ to determine the stress distribution within the granular mass depicted in Figure 1(b). These solutions apply to the limiting idealized Coulomb-Mohr theory of “highly frictional” granular solids, for which we make the following additional comments. Firstly, for $\phi = \pi/2$ the two families of generally distinct slip-planes coincide. Secondly, we observe from the Coulomb-Mohr yield condition (1) that while $\tan \phi$ tends to infinity as ϕ tends to $\pi/2$, along the yield surface the normal component σ tends to zero in such a manner that the product remains finite. Physically, this is equivalent to slip occurring along a surface with infinite friction, a phenomena which is known but often not properly understood (see Lynch and Mason [23, 24]). We emphasize that under such circumstances the assumption of $\phi = \pi/2$ does not correspond to a perfectly rough material where infinite friction prohibits any relative movement of contacting particles. We also observe that as ϕ tends to $\pi/2$, the maximum principal stress (given by $\sigma_I = -p + q$ where p and q are the stress invariants defined by (4)) tends to zero.

We further comment that as ϕ tends to $\pi/2$, then in terms of the Cauchy stresses the limiting yield condition (1) becomes $\sigma_{xy}^2 = \sigma_{xx}\sigma_{yy}$ and $\sigma_{rz}^2 = \sigma_{rr}\sigma_{zz}$, for two and three-dimensional geometries respectively. We observe that these conditions happen to also be the natural conditions underlying all free surface problems, in the sense that the Cauchy stresses on any free surface must satisfy (50) and (67), which are only meaningful provided $\sigma_{xy}^2 - \sigma_{xx}\sigma_{yy}$ and $\sigma_{rz}^2 - \sigma_{rr}\sigma_{zz}$ vanish along the free surface, for two and three-dimensions respectively. As a result, the special case of the angle of internal friction equal to ninety degrees is reasonable as an initial approach for any problem that possesses a free surface. Furthermore, if we assume these conditions are satisfied throughout the entire material, as is the case for $\phi = \pi/2$, then any valid solution has potential free surfaces at any point throughout the entire material.

For $\phi = \pi/2$, we may show from (50) and (67) that the slip-planes and potential free surfaces within the material coincide. We may imagine that as ϕ increases towards $\pi/2$, the slip-planes coalesce and simultaneously the normal stress and tangential shear to these surfaces decrease in magnitude, to the extent of vanishing in the actual limit of $\phi = \pi/2$, so effectively the slip-planes become traction free. We comment that this is entirely consistent with equation (1), noting that τ is zero and σ tends to zero in such a way that the limit of $\sigma \tan \phi$ tends to the cohesion c as ϕ tends to $\pi/2$. With $\phi = \pi/2$ and $p = q$, this follows from the relations $\tau = q \cos \phi$ and $\sigma = q \sin \phi - p$ (see Spencer [25]), which satisfy (1) as an equality and give rise to (6).

In the following section, we state briefly the basic equations of the continuum mechanical theory of granular solids for quasi-static flow of a material which satisfies the Coulomb-Mohr yield condition, for both two and three dimensional rat-holes. In Section 3, we summarize the known exact analytical parametric solutions of the governing equations for two and three dimensions, and these solutions are applied to the rat-hole problem in Section 4. The stress profiles corresponding to these solutions are shown graphically in Section 5. Finally, we note that in previous papers (Hill and Cox [15, 16, 17] and Cox and Hill [18]) we have followed the notation of Spencer and Bradley [26], who adopt the unusual convention of the x -axis being vertical in the two-dimensional situation. However, in this paper we adopt the more usual approach of the x -axis being horizontal. Because the relationship between the parametric solutions in these previous papers and those stated here is by no means obvious, for completeness some details are presented in the Appendix.

2 Basic equations for two and three dimensions

In the following two subsections we briefly state the two and three-dimensional basic equations for the continuum mechanical theory of granular solids for quasi-static gravity flow. We then apply these equations to the industrial granular problem

of determining the stress distribution within an existing static rat-hole, which is valid provided we assume the material throughout the entire rat-hole is at the point of yield. As such, we assume that the material satisfies the Coulomb-Mohr yield condition

$$|\tau| \leq c - \sigma \tan \phi, \quad (1)$$

where c is the cohesion, ϕ is a material constant referred to as the angle of internal friction, and σ and τ denote the normal component of compressive traction and the tangential component of traction respectively. We note that equality only holds in (1) when the granular material is at yield.

2.1 Two-dimensional basic equations

In terms of the rectangular Cartesian coordinates (x, y) as defined in Figure 3(a), the nonzero Cauchy stress components for quasi-static plane strain flow satisfy the equilibrium equations

$$\frac{\partial \sigma_{xx}}{\partial x} + \frac{\partial \sigma_{xy}}{\partial y} = 0, \quad \frac{\partial \sigma_{xy}}{\partial x} + \frac{\partial \sigma_{yy}}{\partial y} = \rho g, \quad (2)$$

where ρ denotes the bulk density, assumed constant, g is acceleration due to gravity, and σ_{xx} , σ_{xy} and σ_{yy} denote the usual in-plane Cauchy stress components, which are assumed to be positive in tension, namely the usual convention in continuum mechanics is adopted that positive forces are assumed to produce positive extensions. These components may be expressed in the standard form

$$\sigma_{xx} = -p + q \cos 2\psi, \quad \sigma_{yy} = -p - q \cos 2\psi, \quad \sigma_{xy} = q \sin 2\psi, \quad (3)$$

where p and q are the quantities defined by

$$p = -\frac{1}{2}(\sigma_{xx} + \sigma_{yy}), \quad q = \frac{1}{2} \left\{ (\sigma_{xx} - \sigma_{yy})^2 + 4\sigma_{xy}^2 \right\}^{1/2}, \quad (4)$$

while the stress angle ψ is given by

$$\tan 2\psi = \frac{2\sigma_{xy}}{\sigma_{xx} - \sigma_{yy}}, \quad (5)$$

and physically ψ is the angle between the maximum principal stress axis and the positive x direction, in the direction of increasing θ . We note that θ is defined by Figure 3(a), and in general, p and q are positive. From the above relations we find that the Coulomb-Mohr yield condition can be expressed in the form

$$q = p \sin \phi + c \cos \phi, \quad (6)$$

which upon substituting into (3) gives

$$\begin{aligned} \sigma_{xx} &= q(\cos 2\psi - \operatorname{cosec} \phi) + c \cot \phi, \\ \sigma_{yy} &= -q(\cos 2\psi + \operatorname{cosec} \phi) + c \cot \phi, \\ \sigma_{xy} &= q \sin 2\psi. \end{aligned} \quad (7)$$

We find that upon substituting (7) into the equilibrium equations (2), and solving for q_x and q_y , we find

$$q_x = \frac{\beta}{\beta^2 - 1} \{ \rho g \beta \sin 2\psi + 2q [\psi_x \sin 2\psi - \psi_y (\beta + \cos 2\psi)] \}, \quad (8)$$

$$q_y = \frac{\beta}{\beta^2 - 1} \{ \rho g (1 - \beta \cos 2\psi) + 2q [\psi_x (\beta - \cos 2\psi) - \psi_y \sin 2\psi] \},$$

where $\beta = \sin \phi$.

From (8) it is clear that the values $\beta = \pm 1$ give rise to special cases. Upon rewriting (8) in the form

$$(\beta - 1)(q_x \cos \psi + q_y \sin \psi) = \rho g \beta \sin \psi + 2\beta q(\psi_x \sin \psi - \psi_y \cos \psi), \quad (9)$$

$$(\beta + 1)(q_x \sin \psi - q_y \cos \psi) = \rho g \beta \cos \psi - 2\beta q(\psi_x \cos \psi + \psi_y \sin \psi),$$

then for the special case of $\beta = 1$, (9)₁ gives q explicitly as

$$q = -\frac{\rho g}{2} \frac{1}{(\psi_x - \psi_y \cot \psi)}. \quad (10)$$

From (9)₂ for $\beta = 1$, we find

$$2(q \sin \psi)_x = \rho g \cos \psi + 2(q \cos \psi)_y, \quad (11)$$

which upon substituting (10) into (11) and simplifying, gives rise to the curious nonlinear partial differential equation

$$h_{xx} - 2hh_{xy} + h^2h_{yy} = 0, \quad (12)$$

where $h = \cot \psi$. We observe that in the other special case $\beta = -1$, which is nonphysical, we may deduce (12) in a similar manner where $h = -\tan \psi$, but this case will not be considered here.

We note that equations (9) can be rewritten as

$$\begin{aligned} & \rho g \sin \psi + 2q(\psi_x \sin \psi - \psi_y \cos \psi) \\ &= (1 - \beta) [\rho g \sin \psi - q_x \cos \psi - q_y \sin \psi + 2q(\psi_x \sin \psi - \psi_y \cos \psi)], \end{aligned} \quad (13)$$

$$\begin{aligned} & \rho g \cos \psi - 2(q \sin \psi)_x + 2(q \cos \psi)_y \\ &= (1 - \beta) [\rho g \cos \psi - q_x \sin \psi + q_y \cos \psi - 2q(\psi_x \cos \psi + \psi_y \sin \psi)]. \end{aligned}$$

In this form it is clear these equations admit perturbation solutions of the form

$$\psi = \psi_0(x, y) + \varepsilon \psi_1(x, y) + O(\varepsilon^2), \quad q = q_0(x, y) + \varepsilon q_1(x, y) + O(\varepsilon^2), \quad (14)$$

where $\varepsilon = 1 - \beta$, with (14) satisfying (10) and (11) to leading order.

We also comment that for any free surface within the material $f(x, y) = \text{constant}$, we have upon differentiating with respect to x

$$f_x + f_y \frac{dy}{dx} = 0, \quad (15)$$

and therefore

$$\frac{dy}{dx} = -\frac{f_x}{f_y} = -\frac{n_x}{n_y}, \quad (16)$$

since the unit normal $\mathbf{n} = (n_x, n_y)$ to the free surface has components given by

$$n_x = \frac{f_x}{(f_x^2 + f_y^2)^{1/2}}, \quad n_y = \frac{f_y}{(f_x^2 + f_y^2)^{1/2}}. \quad (17)$$

Thus, from (3), (6), (16) and (50) we may deduce for the special case of $\phi = \pi/2$ that $dy/dx = -\cot \psi$, which is also the equation for the slip-planes.

2.2 Three-dimensional basic equations

In terms of the cylindrical polar coordinates (r, z) as defined in Figure 3(b) and following Hill and Wu [27], the nonzero stress components for quasi-static axially symmetric flow satisfy the equilibrium equations

$$\frac{\partial \sigma_{rr}}{\partial r} + \frac{\partial \sigma_{rz}}{\partial z} + \frac{\sigma_{rr} - \sigma_{\varphi\varphi}}{r} = 0, \quad \frac{\partial \sigma_{rz}}{\partial r} + \frac{\partial \sigma_{zz}}{\partial z} + \frac{\sigma_{rz}}{r} = \rho g, \quad (18)$$

where ρ denotes the bulk density, assumed constant, g is acceleration due to gravity, and $\sigma_{rr}, \sigma_{zz}, \sigma_{rz}$ and $\sigma_{\varphi\varphi}$ denote the usual physical Cauchy stress components, which are assumed to be positive in tension. We note that $\sigma_{\varphi\varphi}$ is called the hoop stress, where φ is the angular direction around the vertical z axis. We also note that while we are considering a three-dimensional rat-hole, the assumption of axial symmetry around the z axis essentially reduces the equations to only two-dimensions. Again, the stress components can be expressed in the standard form

$$\sigma_{rr} = -p + q \cos 2\psi, \quad \sigma_{zz} = -p - q \cos 2\psi, \quad \sigma_{rz} = q \sin 2\psi, \quad (19)$$

where p and q are the quantities defined by

$$p = -\frac{1}{2}(\sigma_{rr} + \sigma_{zz}), \quad q = \frac{1}{2} \left\{ (\sigma_{rr} - \sigma_{zz})^2 + 4\sigma_{rz}^2 \right\}^{1/2}, \quad (20)$$

while the stress angle ψ is given by

$$\tan 2\psi = \frac{2\sigma_{rz}}{\sigma_{rr} - \sigma_{zz}}, \quad (21)$$

and physically ψ is the angle between the maximum principal stress axis and the r direction, in the direction of decreasing θ . We note that θ is defined by Figure 3(b), and in general, p and q are positive quantities.

Now, we need to make an assumption about the hoop stress in order to determine an expression for $\sigma_{\varphi\varphi}$ in terms of p, q and ψ . Cox *et al.* [28] state that the plastic regimes which agree with the Haar-von Karman hypothesis are likely to be of the greatest significance in the solution of problems of interest. The heuristic Haar-von Karman principle states, under an axially symmetric condition, that the hoop stress

is equal to either the maximum or minimum principal stress. This gives rise to the notion of the Haar-von Karman regimes, and in particular, $\sigma_I = \sigma_{\varphi\varphi} = \sigma_{II} > \sigma_{III}$, where σ_I, σ_{II} and σ_{III} denote the maximum, intermediate and minimum principal stresses respectively. Thus, we may deduce

$$\sigma_{\varphi\varphi} = -p + q. \quad (22)$$

We again note that the above equations describe quasi-static gravity flow, which we are utilizing to determine the stress distribution within an existing static rat-hole. This approach is valid provided we assume that the entire material is at the point of yield. As such, we assume that the equality of the Coulomb-Mohr yield condition is satisfied throughout the entire material, which from the above relations can be expressed in the form

$$q = p \sin \phi + c \cos \phi, \quad (23)$$

so that upon substituting into (19) and (22) gives

$$\begin{aligned} \sigma_{rr} &= q(\cos 2\psi - \operatorname{cosec} \phi) + c \cot \phi, \\ \sigma_{zz} &= -q(\cos 2\psi + \operatorname{cosec} \phi) + c \cot \phi, \\ \sigma_{rz} &= q \sin 2\psi, \\ \sigma_{\varphi\varphi} &= q(1 - \operatorname{cosec} \phi) + c \cot \phi. \end{aligned} \quad (24)$$

We find that upon substituting (24) into the equilibrium equations (18), and solving for q_r and q_z gives

$$\begin{aligned} q_r &= \frac{\beta}{\beta^2 - 1} \{ \rho g \beta \sin 2\psi + 2q [\psi_r \sin 2\psi - \psi_z (\beta + \cos 2\psi)] \\ &\quad + q(\beta - 1)(\cos 2\psi - 1)/r \}, \end{aligned} \quad (25)$$

$$\begin{aligned} q_z &= \frac{\beta}{\beta^2 - 1} \{ \rho g (1 - \beta \cos 2\psi) + 2q [\psi_r (\beta - \cos 2\psi) - \psi_z \sin 2\psi] \\ &\quad + q(\beta - 1) \sin 2\psi / r \}, \end{aligned}$$

where $\beta = \sin \phi$.

From (25) it is again clear that the values $\beta = \pm 1$ give rise to special cases. Upon rewriting (25) in the form

$$(\beta - 1)(q_r \cos \psi + q_z \sin \psi) = \rho g \beta \sin \psi + 2\beta q(\psi_r \sin \psi - \psi_z \cos \psi), \quad (26)$$

$$(\beta + 1)(q_r \sin \psi - q_z \cos \psi) = \rho g \beta \cos \psi - 2\beta q \left(\psi_r \cos \psi + \psi_z \sin \psi + \frac{1}{r} \sin \psi \right),$$

then for the special case of $\beta = 1$, (26)₁ gives q explicitly as

$$q = -\frac{\rho g}{2} \frac{1}{(\psi_r - \psi_z \cot \psi)}. \quad (27)$$

Similarly, from (26)₂ for $\beta = 1$, we find

$$2(q \sin \psi)_r = \rho g \cos \psi + 2(q \cos \psi)_z - \frac{2q}{r} \sin \psi, \quad (28)$$

which upon substituting (27) into (28) and simplifying, gives

$$h_{rr} - 2hh_{rz} + h^2 h_{zz} - \frac{1}{r}(h_r - hh_z) = 0, \quad (29)$$

where $h = \cot \psi$. We observe that in the other special case $\beta = -1$, which is non-physical, we may deduce (29) in a similar manner where $h = -\tan \psi$ and assuming $\sigma_{\varphi\varphi} = -p - q$, which arises from the Haar-von Karman regime corresponding to the stress state $\sigma_I > \sigma_{II} = \sigma_{\varphi\varphi} = \sigma_{III}$, but this case will not be considered here.

We note that equations (26) can be rewritten as

$$\begin{aligned} & \rho g \sin \psi + 2q(\psi_r \sin \psi - \psi_z \cos \psi) \\ &= (1 - \beta) [\rho g \sin \psi - q_r \cos \psi - q_z \sin \psi + 2q(\psi_r \sin \psi - \psi_z \cos \psi)], \end{aligned} \quad (30)$$

$$\begin{aligned} & \rho g \cos \psi - 2(q \sin \psi)_r + 2(q \cos \psi)_z - \frac{2q}{r} \sin \psi \\ &= (1 - \beta) \left[\rho g \cos \psi - q_r \sin \psi + q_z \cos \psi - 2q \left(\psi_r \cos \psi + \psi_z \sin \psi + \frac{1}{r} \sin \psi \right) \right]. \end{aligned}$$

In this form it is clear these equations admit perturbation solutions of the form

$$\psi = \psi_0(r, z) + \varepsilon \psi_1(r, z) + O(\varepsilon^2), \quad q = q_0(r, z) + \varepsilon q_1(r, z) + O(\varepsilon^2), \quad (31)$$

where $\varepsilon = 1 - \beta$, with (31) satisfying (27) and (28) to leading order.

3 Exact analytical solutions

In the following two subsections we summarize the exact parametric solutions of the governing equations for an idealized granular solid with an angle of internal friction equal to ninety degrees, which we utilize to determine stress distributions in two and three-dimensional rat-holes.

3.1 Two-dimensional exact parametric solution

Upon making a substitution of the form $h(x, y) = K(\xi)$, where $\xi = x/y$, we find that (12) becomes

$$K'' + 2K(K' + \xi K'') + K^2\xi(2K' + \xi K'') = 0, \quad (32)$$

where the prime denotes differentiation with respect to ξ . Now, this equation remains invariant under the stretching transformation $\xi_1 = e^\epsilon \xi, K_1 = e^{-\epsilon} K$, and therefore we introduce the new variable $\kappa = \xi K$, so that upon making the Euler transformation $t = \ln \xi$, (32) becomes

$$\kappa_{tt} - \kappa_t - \frac{2}{1 + \kappa} (\kappa_t - \kappa) = 0. \quad (33)$$

Now, as was first shown in Hill and Cox [15], the exact parametric solution of (33) becomes

$$2s^{-1/2}e^{s/2} - I(s) = \frac{C_2}{\xi}, \quad (34)$$

where $s = \kappa_t - \kappa$, the integral $I(s)$ is defined by

$$I(s) = \int^s \omega^{-1/2} e^{\omega/2} d\omega + C_1, \quad (35)$$

and C_1 and C_2 denote arbitrary constants of integration. Further, Hill and Cox [15] show that

$$\kappa = I(s) \left\{ 2s^{-1/2}e^{s/2} - I(s) \right\}^{-1}, \quad (36)$$

so that as $\kappa = \xi K$, then clearly

$$K = \frac{I(s)}{C_2}. \quad (37)$$

Therefore, from (34) and (37) we find

$$\tan \theta = \frac{2s^{-1/2}e^{s/2} - I(s)}{C_2}, \quad \cot \psi = \frac{I(s)}{C_2}. \quad (38)$$

In order to determine a relation for q in terms of the parameter s , we rewrite (10) in the form

$$q = \frac{\rho gr}{2} \frac{\sec \theta}{(\cot \psi + \tan \theta)\psi_\theta}, \quad (39)$$

so that upon differentiating (38), we find that (39) becomes

$$q = \frac{\rho gr}{4} \frac{s^{-1/2}e^{-s/2} [C_2^2 + I^2(s)]}{\{C_2^2 + [2s^{-1/2}e^{s/2} - I(s)]^2\}^{1/2}}, \quad (40)$$

and (38) and (40) constitutes as an exact solution of (10) and (12) for $\beta = 1$.

3.2 Axially symmetric exact parametric solution

Upon making a substitution of the form $h(r, z) = K(\xi)$, where $\xi = r/z$, we find that (29) becomes

$$\xi K'' - K' + K\xi(K' + 2\xi K'') + K^2\xi^2(2K' + \xi K'') = 0, \quad (41)$$

where the prime denotes differentiation with respect to ξ . Now this equation also remains invariant under the same stretching transformation $\xi_1 = e^\epsilon \xi$, $K_1 = e^{-\epsilon} K$, and therefore we again introduce the new variable $\kappa = \xi K$, so that upon making the Euler transformation $t = \ln \xi$, (41) becomes

$$\kappa_{tt} - \kappa_t - \frac{3}{1 + \kappa}(\kappa_t - \kappa) = 0. \quad (42)$$

Now, as was first shown in Cox and Hill [18], the exact parametric solution of (42) becomes

$$3s^{-1/3}e^{s/3} - I(s) = \frac{C_2}{\xi}, \quad (43)$$

where $s = \kappa_t - \kappa$, the integral $I(s)$ is defined by

$$I(s) = \int^s \omega^{-1/3} e^{\omega/3} d\omega + C_1, \quad (44)$$

and C_1 and C_2 denote arbitrary constants of integration. Further, as shown in Cox and Hill [18]

$$\kappa = I(s) \left\{ 3s^{-1/3} e^{s/3} - I(s) \right\}^{-1}, \quad (45)$$

so that as $\kappa = \xi K$, then clearly

$$K = \frac{I(s)}{C_2}. \quad (46)$$

Thus, from (43) and (46) we find

$$\cot \theta = \frac{3s^{-1/3} e^{s/3} - I(s)}{C_2}, \quad \cot \psi = \frac{I(s)}{C_2}. \quad (47)$$

In order to determine a relation for q in terms of the parameter s , we rewrite (27) in the form

$$q = -\frac{\rho g R}{2} \frac{\operatorname{cosec} \theta}{(\cot \psi + \cot \theta) \psi_\theta}, \quad (48)$$

where R is as defined in Figure 3 and upon differentiating (47), we find that (48) becomes

$$q = \frac{\rho g R}{6} \frac{s^{-2/3} e^{-s/3} [C_2^2 + I^2(s)]}{\{C_2^2 + [3s^{-1/3} e^{s/3} - I(s)]^2\}^{1/2}}, \quad (49)$$

and (47) and (49) constitutes as an exact solution of (27) and (29) for $\beta = 1$.

4 The rat-hole problem

In this section we apply the two and three-dimensional exact parametric solutions to the problem of determining stress profiles in an existing defined rat-hole with profile shown in Figure 1(b).

4.1 Two-dimensional rat-holes

In order to exploit the two-dimensional exact parametric solution, (38) and (40), to determine stress profiles in two-dimensional vertical channel rat-holes with an infinitesimal central outlet and a sloping rigid base, we first need to determine the appropriate boundary conditions. We note that due to the assumed geometry of the

rat-hole, with coordinates system as shown in Figure 3(a), we see that the rat-hole is symmetric about the vertical axis, so we only need to consider $0 \leq \theta \leq \pi/2$. Now, for the stress free conditions along the upper surface of the rat-hole, we require both the horizontal and vertical stresses to vanish, namely

$$\sigma_x = \sigma_{xx}n_x + \sigma_{xy}n_y = 0, \quad \sigma_y = \sigma_{xy}n_x + \sigma_{yy}n_y = 0, \quad (50)$$

where n_x and n_y denote the corresponding components of the normal to the surface. Thus, from (3) and assuming $q(\gamma) \neq 0$, we find on the upper sloping surface given by $\theta = \gamma$ that $\cos[\psi - \gamma] = 0$, which clearly gives rise to the boundary condition

$$\psi(\gamma) = \gamma \pm \frac{\pi}{2}. \quad (51)$$

We note that at $\theta = \gamma$, (50) can be shown to be equivalent to

$$\sigma_{rr} = \frac{\sigma_{xy}}{\sin \gamma \cos \gamma}, \quad \sigma_{\theta\theta} = 0, \quad \sigma_{r\theta} = 0, \quad (52)$$

where r and θ are defined by Figure 3(a). To do this, we first note from Hunter [29] (page 102) that the cylindrical stresses may be expressed in terms of the Cartesian stresses as

$$\begin{aligned} \sigma_{rr} &= \sigma_{xx} \cos^2 \theta + 2\sigma_{xy} \sin \theta \cos \theta + \sigma_{yy} \sin^2 \theta, \\ \sigma_{\theta\theta} &= \sigma_{xx} \sin^2 \theta - 2\sigma_{xy} \sin \theta \cos \theta + \sigma_{yy} \cos^2 \theta, \\ \sigma_{r\theta} &= (\sigma_{yy} - \sigma_{xx}) \sin \theta \cos \theta + \sigma_{xy} \cos 2\theta. \end{aligned} \quad (53)$$

Also, from (4) and (6) we find that the Coulomb-Mohr yield condition for the special case of $\beta = 1$ becomes

$$\sigma_{xy}^2 = \sigma_{xx}\sigma_{yy}, \quad (54)$$

so that (53) and (54) gives

$$\begin{aligned} \sigma_{rr} &= \sigma_{xy} \left[\frac{\sigma_{xy}}{\sigma_{yy}} \cos^2 \theta + \frac{\sigma_{xy}}{\sigma_{xx}} \sin^2 \theta + \sin 2\theta \right], \\ \sigma_{\theta\theta} &= \sigma_{xy} \left[\frac{\sigma_{xy}}{\sigma_{yy}} \sin^2 \theta + \frac{\sigma_{xy}}{\sigma_{xx}} \cos^2 \theta - \sin 2\theta \right], \\ \sigma_{r\theta} &= \sigma_{xy} \left[\left(\frac{\sigma_{xy}}{\sigma_{xx}} - \frac{\sigma_{xy}}{\sigma_{yy}} \right) \sin \theta \cos \theta + \cos 2\theta \right], \end{aligned} \quad (55)$$

which are valid for all $0 \leq \theta \leq \gamma$. Finally, if we consider the stress free surface along $\theta = \gamma$, then from (50) we find that

$$\frac{\sigma_{xy}}{\sigma_{xx}} = \tan \gamma, \quad \frac{\sigma_{xy}}{\sigma_{yy}} = \cot \gamma, \quad (56)$$

so that (55) becomes simply (52). Now, to determine the second boundary condition, we assume a Coulomb friction condition along the sloping rigid base $\theta = \alpha$, such that

$$\sigma_{r\theta} = \sigma_{\theta\theta} \tan \mu, \quad (57)$$

where μ is the angle of surface friction. Thus, from (7) and either (53) or (55), we find that provided $q(\alpha) \neq 0$, then (57) becomes $\tan(\psi - \alpha) = -\tan \mu$, which gives rise to the second boundary condition

$$\psi(\alpha) = \alpha - \mu. \quad (58)$$

Now, to apply the boundary conditions (51) and (58) to the two-dimensional exact parametric solution (38) and (40), we find that upon associating the parameter value $s = s_0$ with $\theta = \gamma$, then (38)₁ gives

$$C_2 = [2s_0^{-1/2}e^{s_0/2} - I(s_0)] \cot \gamma, \quad (59)$$

so that (38)₂ becomes

$$\cot \psi = \frac{I(s_0)}{[2s_0^{-1/2}e^{s_0/2} - I(s_0)] \cot \gamma}, \quad (60)$$

from which it is clear to see that in order for (51) to be satisfied, we require $s_0 = -\infty$.

Accordingly, we change the parameter from s to $-\lambda$ and make the substitution $\omega = -t$ in the integral (35). Thus, (38) and (40) becomes

$$\tan \theta = \frac{2\lambda^{-1/2}e^{-\lambda/2} + J(\lambda)}{C_4}, \quad \cot \psi = -\frac{J(\lambda)}{C_4}, \quad (61)$$

$$q = \frac{\rho gr}{4} \frac{\lambda^{-1/2}e^{\lambda/2}[C_4^2 + J^2(\lambda)]}{\{C_4^2 + [2\lambda^{-1/2}e^{-\lambda/2} + J(\lambda)]^2\}^{1/2}},$$

where $C_4 = iC_2$ and the integral $J(\lambda)$ is defined by

$$J(\lambda) = \int^{\lambda} t^{-1/2} e^{-t/2} dt + C_3, \quad (62)$$

where $C_1 = iC_3$. Since $\lambda = \infty$ is the parameter value corresponding to $\theta = \gamma$, we require an estimate of $J(\infty)$. Upon defining C_5 such that

$$J(\lambda) = \int_0^{\lambda} t^{-1/2} e^{-t/2} dt + C_5 = (2\pi)^{1/2} \operatorname{erf}(\lambda/2)^{1/2} + C_5, \quad (63)$$

then clearly $J(\infty) = (2\pi)^{1/2} + C_5$, where erf denotes the usual error function. Thus, at $\theta = \gamma$ we find that $(61)_1$ gives

$$C_4 = [(2\pi)^{1/2} + C_5] \cot \gamma, \quad (64)$$

which upon substituting into $(61)_2$, shows that (51) is satisfied.

Now, in order to satisfy the second boundary condition (58) , we associate the parameter value $\lambda = \lambda_1$ with $\theta = \alpha$, so that from $(61)_1$, (63) and (64) , we find

$$C_5 = \frac{\sqrt{2\pi} \cot \gamma - [2\lambda_1^{-1/2} e^{-\lambda_1/2} + \sqrt{2\pi} \operatorname{erf}(\lambda_1/2)^{1/2}] \cot \alpha}{(\cot \alpha - \cot \gamma)}, \quad (65)$$

which is an equation for the constant of integration C_5 in terms of λ_1 . Finally, from $(61)_2$, we get

$$\lambda_1^{1/2} e^{\lambda_1/2} \operatorname{erfc}(\lambda_1/2)^{1/2} = \left(\frac{2}{\pi}\right)^{1/2} \frac{\cot \alpha [1 + \cot \gamma \cot(\alpha - \mu)]}{\cot \gamma [1 + \cot \alpha \cot(\alpha - \mu)]}, \quad (66)$$

which is a transcendental equation for the determination of the parameter λ_1 , where erfc denotes the usual complementary error function. Thus, the exact parametric solution for a two-dimensional vertical channel rat-hole with an infinitesimal central outlet, for the special case of an angle of internal friction equal to ninety degrees, is given by (61) , (63) and (64) , where λ_1 satisfies (66) and C_5 is given by (65) .

4.2 Three-dimensional rat-holes

In order to exploit the three-dimensional exact parametric solution, (47) and (49) , to determine stress profiles in three-dimensional cylindrical cavity rat-holes with an

infinitesimal central outlet and a sloping rigid base, we first need to determine the appropriate boundary conditions. We note that due to the assumed axial symmetry of the rat-hole, we only need to consider $0 \leq \theta \leq \pi/2$. Now, following the two-dimensional solution, for stress free conditions along the upper surface of the rat-hole, we require both the horizontal and vertical stresses to vanish, namely

$$\sigma_r = \sigma_{rr}n_r + \sigma_{rz}n_z = 0, \quad \sigma_z = \sigma_{rz}n_r + \sigma_{zz}n_z = 0, \quad (67)$$

where n_r and n_z denote the corresponding components of the normal to the surface. Thus, from (19) and assuming $q(\gamma) \neq 0$, we find on the upper sloping surface given by $\theta = \gamma$ that $\sin[\psi + \gamma] = 0$, which clearly gives rise to the boundary condition

$$\psi(\gamma) = -\gamma. \quad (68)$$

We note that at $\theta = \gamma$, (67) can be shown to be equivalent to

$$\sigma_{RR} = \frac{\sigma_{rz}}{\sin \gamma \cos \gamma}, \quad \sigma_{\theta\theta} = 0, \quad \sigma_{R\theta} = 0, \quad (69)$$

where R and θ are defined by Figure 3(b). To do this, we again note from Hunter [29] (page 102) that the spherical stresses may be expressed in terms of the cylindrical stresses as

$$\begin{aligned} \sigma_{RR} &= \sigma_{zz} \cos^2 \theta + 2\sigma_{rz} \sin \theta \cos \theta + \sigma_{rr} \sin^2 \theta, \\ \sigma_{\theta\theta} &= \sigma_{zz} \sin^2 \theta - 2\sigma_{rz} \sin \theta \cos \theta + \sigma_{rr} \cos^2 \theta, \\ \sigma_{R\theta} &= (\sigma_{rr} - \sigma_{zz}) \sin \theta \cos \theta + \sigma_{rz} \cos 2\theta. \end{aligned} \quad (70)$$

Also, from (20) and (23) we find that the Coulomb-Mohr yield condition for the special case of $\beta = 1$ becomes

$$\sigma_{rz}^2 = \sigma_{rr}\sigma_{zz}, \quad (71)$$

so that (70) and (71) can be expressed as

$$\begin{aligned} \sigma_{RR} &= \sigma_{rz} \left[\frac{\sigma_{rz}}{\sigma_{rr}} \cos^2 \theta + \frac{\sigma_{rz}}{\sigma_{zz}} \sin^2 \theta + \sin 2\theta \right], \\ \sigma_{\theta\theta} &= \sigma_{rz} \left[\frac{\sigma_{rz}}{\sigma_{rr}} \sin^2 \theta + \frac{\sigma_{rz}}{\sigma_{zz}} \cos^2 \theta - \sin 2\theta \right], \\ \sigma_{R\theta} &= \sigma_{rz} \left[\left(\frac{\sigma_{rz}}{\sigma_{zz}} - \frac{\sigma_{rz}}{\sigma_{rr}} \right) \sin \theta \cos \theta + \cos 2\theta \right], \end{aligned} \quad (72)$$

which are valid for all $0 \leq \theta \leq \gamma$. Finally, if we consider the stress free surface along $\theta = \gamma$, then from (67) we find that

$$\frac{\sigma_{rz}}{\sigma_{zz}} = \tan \gamma, \quad \frac{\sigma_{rz}}{\sigma_{rr}} = \cot \gamma, \quad (73)$$

so that (72) becomes simply (69). Now, to determine the second boundary condition, we assume a Coulomb friction condition along the sloping rigid base $\theta = \alpha$, such that

$$\sigma_{r\theta} = -\sigma_{\theta\theta} \tan \mu, \quad (74)$$

where μ is the angle of surface friction. Thus, from (24) and either (70) or (72), we find that provided $q(\alpha) \neq 0$ then (74) becomes $\cot(\psi + \alpha) = \tan \mu$, which gives rise to the second boundary condition

$$\psi(\alpha) = -\alpha - \mu \pm \frac{\pi}{2}. \quad (75)$$

Now, to apply the boundary conditions (68) and (75) to the three-dimensional exact parametric solution (47) and (49), we associate the parameter value $s = s_0$ with $\theta = \gamma$, then (47)₁ gives

$$C_2 = [3s_0^{-1/3} e^{s_0/3} - I(s_0)] \tan \gamma, \quad (76)$$

so that (47)₂ becomes

$$\cot \psi = \frac{I(s_0)}{[3s_0^{-1/3} e^{s_0/3} - I(s_0)] \tan \gamma}, \quad (77)$$

from which it is clear to see that for (68) to be satisfied, we require $s_0 = -\infty$.

Accordingly, we again change the parameter from s to $-\lambda$ and make the substitution $w = -t$ in the integral (44). Thus, (47) and (49) becomes

$$\cot \theta = \frac{3\lambda^{-1/3} e^{-\lambda/3} + J(\lambda)}{C_4}, \quad \cot \psi = -\frac{J(\lambda)}{C_4}, \quad (78)$$

$$q = \frac{\rho g R}{6} \frac{\lambda^{-2/3} e^{\lambda/3} [C_4^2 + J^2(\lambda)]}{\{C_4^2 + [3\lambda^{-1/3} e^{-\lambda/3} + J(\lambda)]^2\}^{1/2}},$$

where $C_4 = (-1)^{1/3}C_2$, R is defined by Figure 3(b), and the integral $J(\lambda)$ is given by

$$J(\lambda) = \int^\lambda t^{-1/3} e^{-t/3} dt + C_3, \quad (79)$$

where $C_1 = -(-1)^{-1/3}C_3$. Since $\lambda = \infty$ is the parameter value corresponding to $\theta = \gamma$, we require an estimate of $J(\infty)$. Upon defining C_5 such that

$$J(\lambda) = \int_0^\lambda t^{-1/3} e^{-t/3} dt + C_5 = 3^{2/3} \int_0^{\lambda/3} \eta^{-1/3} e^{-\eta} d\eta + C_5, \quad (80)$$

then $J(\infty) = 3^{2/3}\Gamma(2/3) + C_5$, where Γ is the usual gamma function and noting that we have made the substitution $t = 3\eta$ in the integral (80). Thus, at $\theta = \gamma$ we find that (78)₁ gives

$$C_4 = [3^{2/3}\Gamma(2/3) + C_5] \tan \gamma, \quad (81)$$

which upon substituting into (78)₂, shows that (68) is satisfied.

Now, in order to satisfy the second boundary condition (75), we associate the parameter value $\lambda = \lambda_1$ with $\theta = \alpha$, so that from (78)₁, (80) and (81), we find

$$C_5 = \frac{3^{2/3}\Gamma(2/3) \tan \gamma - [3\lambda_1^{-1/3} e^{-\lambda_1/3} + 3^{2/3} \int_0^{\lambda_1/3} \eta^{-1/3} e^{-\eta} d\eta] \tan \alpha}{(\tan \alpha - \tan \gamma)}, \quad (82)$$

which is an equation for the constant of integration C_5 in terms of λ_1 . Finally, from (78)₂, we get

$$\lambda_1^{1/3} e^{\lambda_1/3} \int_{\lambda_1/3}^\infty \eta^{-1/3} e^{-\eta} d\eta = 3^{1/3} \frac{\tan \alpha [1 + \tan \gamma \tan(\alpha + \mu)]}{\tan \gamma [1 + \tan \alpha \tan(\alpha + \mu)]}, \quad (83)$$

which is a transcendental equation for the determination of the parameter λ_1 . Thus, the exact parametric solution for a three-dimensional cylindrical cavity rat-hole with an infinitesimal central outlet, for the special case of an angle of internal friction equal to ninety degrees, is given by (78), (80) and (81), where λ_1 satisfies (83) and C_5 is given by (82).

5 Results and conclusions

In this section, we illustrate graphically the parametric solutions for two-dimensional channel or slot rat-holes and three-dimensional cylindrical cavity rat-holes resting on

a sloping rigid surface. Figure 4 shows the variation of ψ and $q/\rho gr$, with respect to θ , according to the two-dimensional parametric solution (61), for $\alpha = \pi/10$, $\gamma = \pi/3$ and the angle of surface friction $\mu = \pi/6$. The corresponding plane strain stresses are shown in Figure 5, noting that the cylindrical stress $\sigma_{r\theta}$ is included to demonstrate that the alternate boundary condition (52) is satisfied. We observe from Figure 5(a) that the stress component σ_{xx} is infinite on the stress free surface. Figure 6 shows the variation of ψ and $q/\rho gr$, with respect to θ , according to the three-dimensional parametric solution (78), for $\alpha = \pi/3$, $\gamma = \pi/10$ and the angle of surface friction $\mu = \pi/5$. The corresponding axially symmetric stresses are shown in Figure 7, noting that the spherical stress $\sigma_{R\theta}$ is also shown in this figure to demonstrate that the alternate boundary condition (69) is satisfied. We also observe from Figure 7(a) that the stress component σ_{rr} is infinite on the stress free surface.

We have presented the first analytical solutions for the static stress distribution of two and three-dimensional rat-holes, which have geometry as shown in Figure 1(b), for the limiting situation of a highly frictional granular solid assuming an infinitesimal central outlet such that the material is at rest on a sloping rigid base of infinite extent for which a frictional condition applies. These solutions are bona fide exact solutions of the governing equations for a Coulomb-Mohr granular solid, and satisfy the free surface conditions on the sloping upper surface, and a frictional condition along the sloping rigid base. The solutions presented constitute the only known analytical solutions for a realistic rat-hole geometry, other than the classical solution for a perfectly vertical cylindrical cavity. However, as indicated above we find from Figure 5(a) and Figure 7(a) that the stress components σ_{xx} and σ_{rr} are infinite on the stress free surface for the two and three-dimensional exact solutions respectively. These infinite stress components arise as a result of the stress invariant q being infinite on the stress free surface, as shown in Figure 4(b) and Figure 6(b). This makes uncertain the physical applicability of the formal solutions to the physical problem

of determining the stress distribution within a rat-hole.

Acknowledgements

This work is supported by the Australian Research Council, both through the Large Grant Scheme and for providing a Senior Research Fellowship for JMH. This support is gratefully acknowledged. The authors are also grateful for the data given in Table 1 which was provided by Ms. Wendy Halford, Centre for Bulk Solids and Particulate Technologies, University of Wollongong. Finally, the authors are particularly grateful to Dr. Scott McCue for many helpful discussions and for making a number of suggested changes to this paper.

References

- [1] Jenike, A. J.: Gravity flow of bulk solids. Utah Engineering Experiment Station Bulletin. **108** (1962).
- [2] Jenike, A. J.: Gravity flow of solids. Trans. Inst. Chem. Engrs. **40**, 264-471 (1962).
- [3] Jenike, A. J., Yen, B. C.: Slope stability in axial symmetry. Utah Engineering Experiment Station Bulletin. **115** (1962).
- [4] Jenike, A. J., Yen, B. C.: Slope stability in axial symmetry. In: Proc. 5th Symposium on Rock Mechanics, University of Minnesota, May 1962 (Peramon Press, 1963), 689-711(1963).
- [5] Roberts, A. W.: Bulk solids handling: recent developments and future directions. Bulk Solids Handling. **11**, 17-35 (1991).
- [6] Jenike, A. J.: Storage and flow of solids. Utah Engineering Experiment Station Bulletin. **123** (1964).

- [7] Jenike, A. J.: Steady gravity flow of frictional-cohesive solids in converging channels. *J. Appl. Mech.* **31**, 5-11 (1964).
- [8] Jenike, A. J.: Gravity flow of frictional-cohesive solids - Convergence to radial stress fields. *J. Appl. Mech.* **32**, 205-207 (1965).
- [9] Johanson, J. R.: Stress and velocity fields in the gravity flow of bulk solids. *J. Appl. Mech.* **31**, 499-506 (1964).
- [10] Hill, J. M., Cox, G. M.: Cylindrical cavities and classical rat-hole theory occurring in bulk materials. *Int. J. for Numerical and Analytical Methods in Geomechanics.* **24**, 971-990 (2000).
- [11] Hill, J. M., Cox, G. M.: Stress profiles for tapered cylindrical cavities in granular media. *Int. J. for Solids and Structures.* **38**, 3795-3811 (2001).
- [12] Spencer, A. J. M., Bradley, N. J.: Gravity flow of a granular material in compression between vertical walls and through a tapering vertical channel. *Q. J. Mech. Appl. Math.* **45**, 733-746 (1992).
- [13] Spencer, A. J. M., Bradley, N. J.: Gravity flow of granular materials in contracting cylinders and tapered tubes. *Int. J. Engng. Sci.* **40**, 1529-1552 (2002).
- [14] Hill, J. M., Cox, G. M.: Rat-hole stress profiles for shear-index granular materials. *Acta Mechanica.* **155**, 157-172 (2002).
- [15] Hill, J. M., Cox, G. M.: An exact parametric solution for granular flow in a converging wedge. *Zeitschrift fur angewandte Mathematik und Physik (ZAMP).* **52**, 657-668 (2001).
- [16] Hill, J. M., Cox, G. M.: The force distribution at the base of sand-piles. *Developments in Theoretical Geomechanics, The John Booker Memorial Symposium*, (eds. Smith, D. W. and Carter, J. P.), 43-61 (2000).

- [17] Hill, J. M., Cox, G. M.: On the problem of the determination of force distributions in granular heaps using continuum theory. *Q. J. Mech. Appl. Math.* **55**, 655-668 (2002).
- [18] Cox, G. M., Hill, J. M.: Some exact mathematical solutions for granular stock piles and granular flow in hoppers. *Mathematics and Mechanics of Solids*. **8**, 21-50 (2003).
- [19] Australian Standard: Loads on bulk solids containers, Standards Association of Australia. ISBN 0733707335, **AS 3774**, 23 (1996).
- [20] Perkins, S. W.: Non-linear limit analysis for the bearing capacity of highly frictional soils. 2nd Congress on Computing in Civil Engineering, ASCE, Atlanta, 4 June 1995, **1**, 629-636 (1994).
- [21] Perkins, S. W.: Bearing capacity of highly frictional material. *ASTM Geotechnical Testing Journal*. **18**, 450-462(1995).
- [22] Sture, S.: Constitutive issues in soil liquefaction. *Proc. Physics and Mechanics of Soil Liquefaction*, Rotterdam, Balkema, 1999 (edited by Lade, P. V. and Yanamuro, J. A.), 133-143 (1999).
- [23] Lynch, K. M., Mason, M. T.: Pulling by pushing, slip with infinite friction, and perfectly rough surfaces. *Int. Conf. on Robotics and Automation*, IEEE, May 2-6, Atlanta, 1993, **1**, 745-751 (1993).
- [24] Lynch, K. M., Mason, M. T.: Pulling by pushing, slip with infinite friction, and perfectly rough surfaces. *Int. J. of Robotics Research*. **14**, 174-183 (1995).
- [25] Spencer, A. J. M.: Deformation of ideal granular materials. *Mechanics of Solids: The Rodney Hill 60th Anniversary Volume* (edited by Hopkins, H. G. and Sewell, M. J.), Oxford, Pergamon, 607-652 (1982).

- [26] Spencer, A. J. M., Bradley, N. J.: Gravity flow of granular materials in converging wedges and cones, Proc. 8th Int. Sym. Continuum Models and Discrete Systems, Singapore, 11-16th June, 1996 (edited by Markov, K. Z.), 581-590 (1996).
- [27] Hill, J. M., Wu, Y. H.: Some axially symmetric flows of Mohr-Coulomb compressible granular materials. Proc. R. Soc. Lond. **438**, 67-93 (1992).
- [28] Cox, A. D., Eason, G., Hopkins, H. G.: Axially symmetric plastic deformations in soils. Phil. Trans. Roy. Soc. Lond. **A254**, 1-45 (1961).
- [29] Hunter, S. C.: Mechanics of continuum media, Ellis Horwood Limited, **2nd ed.**, 124-125 (1983).

A Appendix A. Correspondence of exact parametric solutions

In previous papers, (Hill and Cox [15, 16, 17] and Cox and Hill [18]), we have followed the notation of Spencer and Bradley [26], who adopt the unusual convention of the x -axis being vertical in the two-dimensional case. In this paper we have adopted the more usual approach of the x -axis being horizontal, and the purpose of this appendix is to detail the relations between the various physical quantities, and in particular, the relationship between the two-dimensional exact parametric solution given in the previous papers and that stated here. The connection between these two solutions is not immediately apparent and for this reason we present the details given below.

As indicated in Figure 8, starred variables denote the quantities used in the previous papers, namely with the x -axis being vertical, whereas unstarred variables are those used in this paper, namely with the x -axis being horizontal. From Hunter [29] (page 124), we find for two fixed rectangular coordinates systems, centered at the

same origin, that the relationship between the coordinates x_i^* and x_j is given by

$$x_i^* = Q_{ij}x_j, \quad (\text{A1})$$

where Q_{ij} denote the components of a proper orthogonal matrix \mathbf{Q} such that $\mathbf{Q}\mathbf{Q}^T = \mathbf{Q}^T\mathbf{Q} = \mathbf{1}$ and $|\mathbf{Q}| = 1$. Hunter [29] (page 125) also states that the corresponding stresses are related by

$$\sigma^* = \mathbf{Q}\sigma\mathbf{Q}^T. \quad (\text{A2})$$

Thus, from Figure 8 it is clear that \mathbf{Q} is given by

$$\mathbf{Q} = \begin{pmatrix} 0 & 1 & 0 \\ 1 & 0 & 0 \\ 0 & 0 & -1 \end{pmatrix}, \quad (\text{A3})$$

so that (A2) becomes

$$\begin{pmatrix} \sigma_{xx}^* & \sigma_{xy}^* & 0 \\ \sigma_{xy}^* & \sigma_{yy}^* & 0 \\ 0 & 0 & \sigma_{zz}^* \end{pmatrix} = \begin{pmatrix} \sigma_{yy} & \sigma_{xy} & 0 \\ \sigma_{xy} & \sigma_{xx} & 0 \\ 0 & 0 & \sigma_{zz} \end{pmatrix}. \quad (\text{A4})$$

Now, from (7) and the corresponding relations in the previous papers, namely

$$\sigma_{rr}^* = q^*(\cos 2\psi^* - 1), \quad \sigma_{\theta\theta}^* = -q^*(\cos 2\psi^* + 1), \quad \sigma_{r\theta}^* = q^* \sin 2\psi^*, \quad (\text{A5})$$

we find that we require the stress decompositions in the previous papers, namely (A5), to be expressed in Cartesian form. From Hunter [29] (page 102), we find

$$\begin{aligned} \sigma_{xx}^* &= \sigma_{rr}^* \cos^2 \theta^* + \sigma_{\theta\theta}^* \sin^2 \theta^* - \sigma_{r\theta}^* \sin 2\theta^*, \\ \sigma_{yy}^* &= \sigma_{\theta\theta}^* \cos^2 \theta^* + \sigma_{rr}^* \sin^2 \theta^* + \sigma_{r\theta}^* \sin 2\theta^*, \\ \sigma_{xy}^* &= \frac{1}{2}(\sigma_{rr}^* - \sigma_{\theta\theta}^*) \sin 2\theta^* + \sigma_{r\theta}^* \cos 2\theta^*, \end{aligned} \quad (\text{A6})$$

so that from (7) and (A4) - (A6) we obtain

$$\begin{aligned} q^* \{\cos[2(\theta^* + \psi^*)] - 1\} &= -q(\cos 2\psi + 1), \\ -q^* \{\cos[2(\theta^* + \psi^*)] + 1\} &= q(\cos 2\psi - 1), \\ q^* \sin[2(\theta^* + \psi^*)] &= q \sin 2\psi. \end{aligned} \quad (\text{A7})$$

Therefore, upon dividing (A7)₃ by (A7)₂, we may deduce

$$\tan(\theta^* + \psi^*) = \cot \psi, \tag{A8}$$

from which we find

$$\theta^* + \psi^* = \frac{\pi}{2} - \psi, \tag{A9}$$

and upon substituting (A9) into (A7), we have $q^* = q$. Also, from Figure 8 it is clear that

$$\theta^* + \theta = \frac{\pi}{2}, \quad r^* = r, \tag{A10}$$

so that altogether the basic relations connecting the two systems are given by (A4), (A9) and (A10) and the actual parameters involved in the two parametric solutions coincide.

Figure Captions

Figure 1. Schematic of a rat-hole geometry ((a) the most common and (b) resting on a rigid plane).

Figure 2. Schematic of mass-flow and funnel-flow in a hopper ((a) mass-flow and (b) funnel-flow).

Figure 3. Coordinates for two and three-dimensional rat-holes with the considered profile ((a) two dimensions and (b) three dimensions).

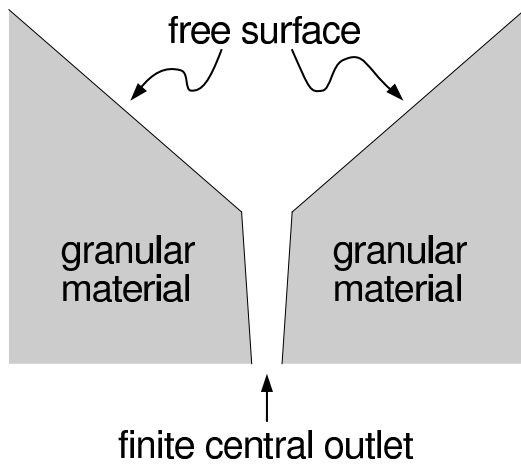
Figure 4. Variation of ψ and $q/\rho gr$ for the two-dimensional exact parametric solution (61). ((a) ψ and (b) $q/\rho gr$).

Figure 5. Variation of the plane strain stresses, as given by (3) and (61). ((a) $\sigma_{xx}/\rho gr$, (b) $\sigma_{xy}/\rho gr$, (c) $\sigma_{yy}/\rho gr$ and (d) $\sigma_{r\theta}/\rho gr$).

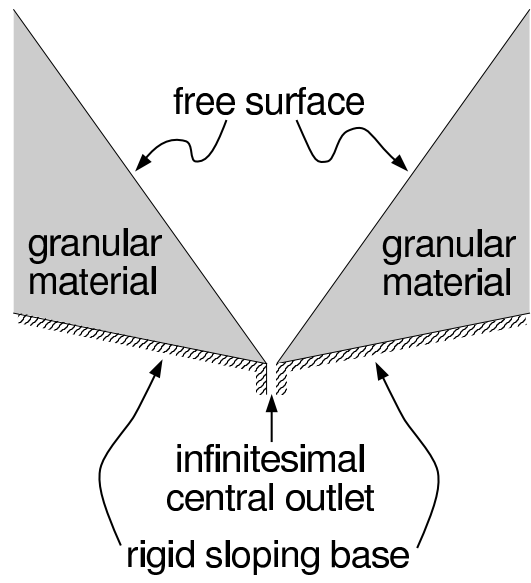
Figure 6. Variation of ψ and $q/\rho gR$ for the three-dimensional exact parametric solution (78). ((a) ψ and (b) $q/\rho gR$).

Figure 7. Variation of the axially symmetric stresses, as given by (19) and (78). ((a) $\sigma_{rr}/\rho gR$, (b) $\sigma_{rz}/\rho gR$, (c) $\sigma_{zz}/\rho gR$ and (d) $\sigma_{R\theta}/\rho gR$).

Figure 8. Coordinates for the two systems used in previous papers and this paper in two dimensions. Stars denote quantities in previous papers ((a) previous papers and (b) this paper).

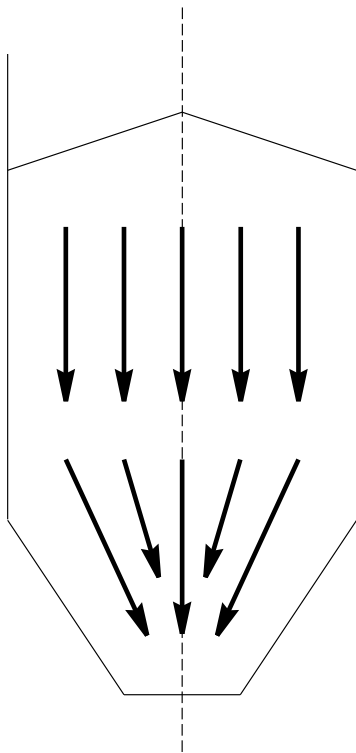


(a).

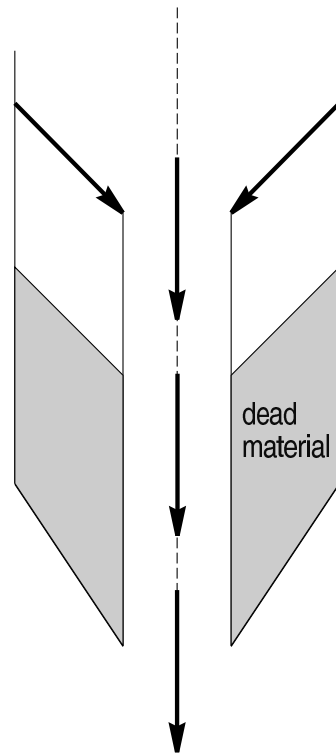


(b).

Figure 1.

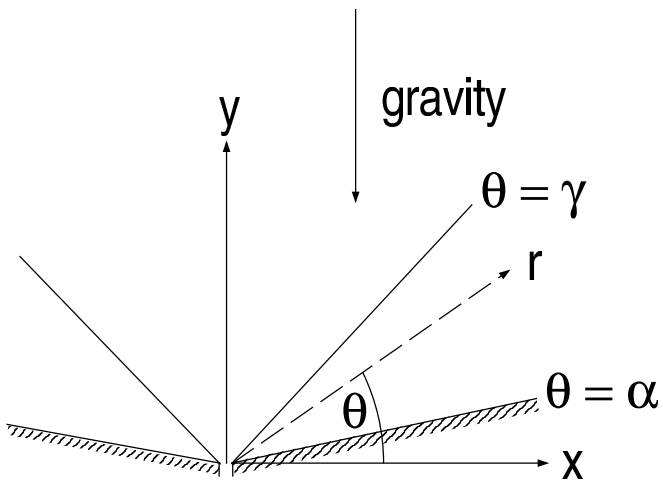


(a).

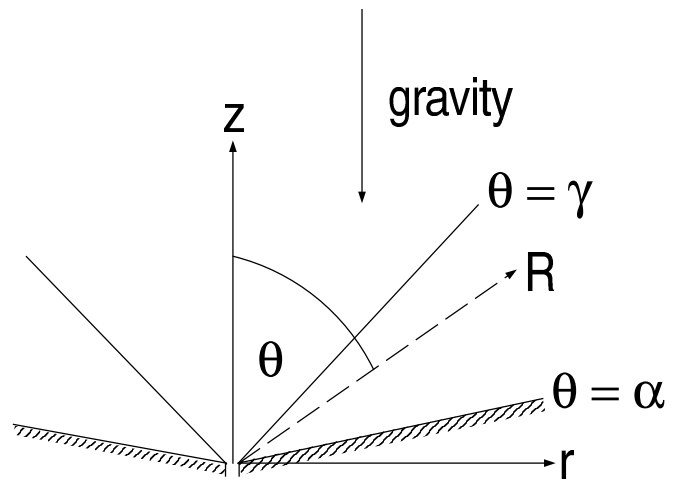


(b).

Figure 2.

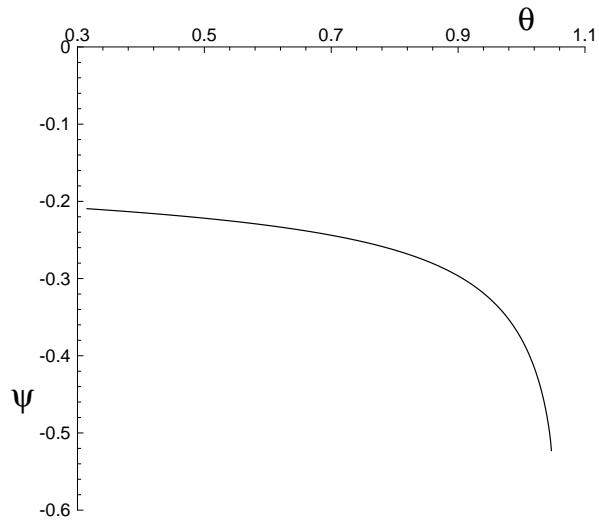


(a).

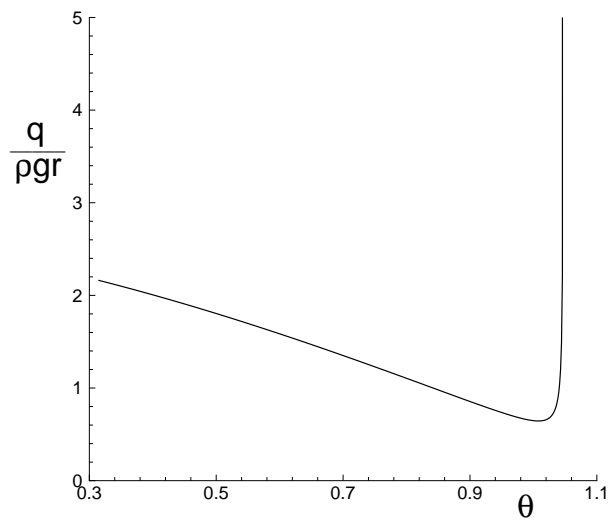


(b).

Figure 3.

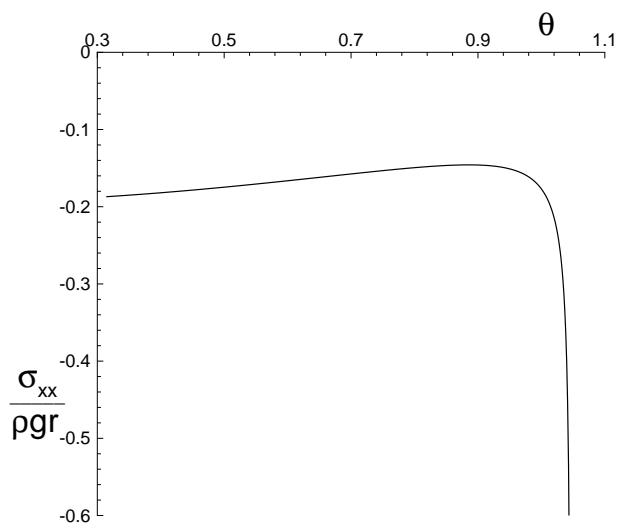


(a).

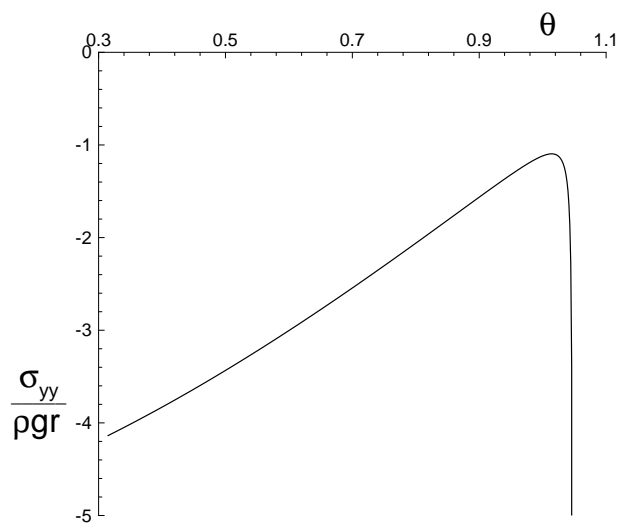


(b).

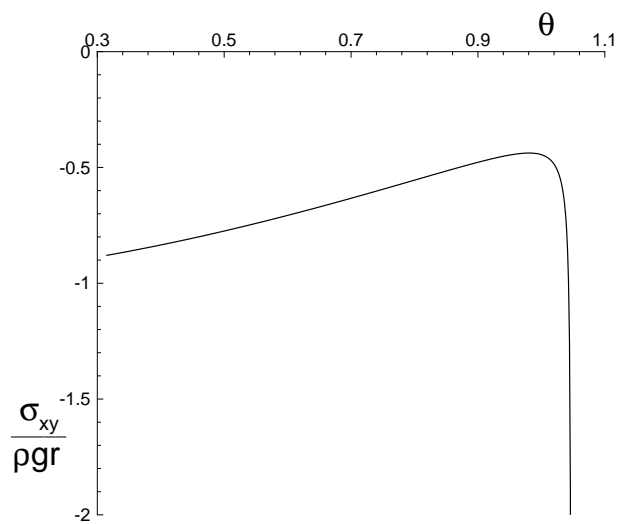
Figure 4.



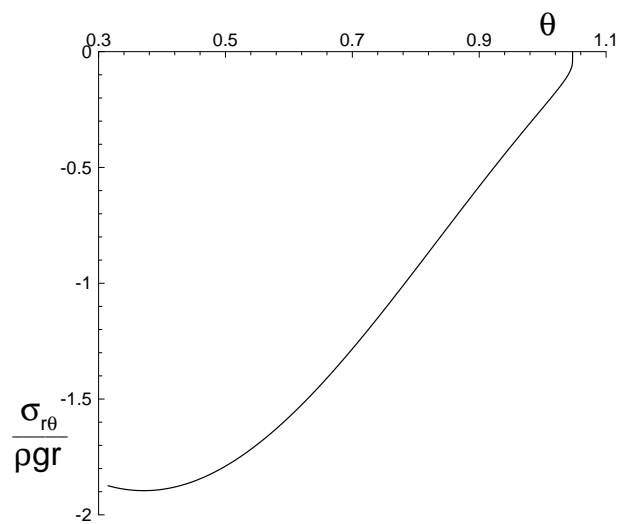
(a).



(b).

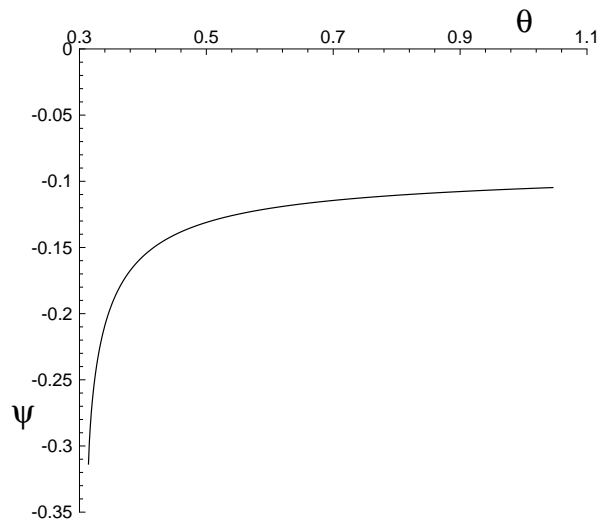


(c).

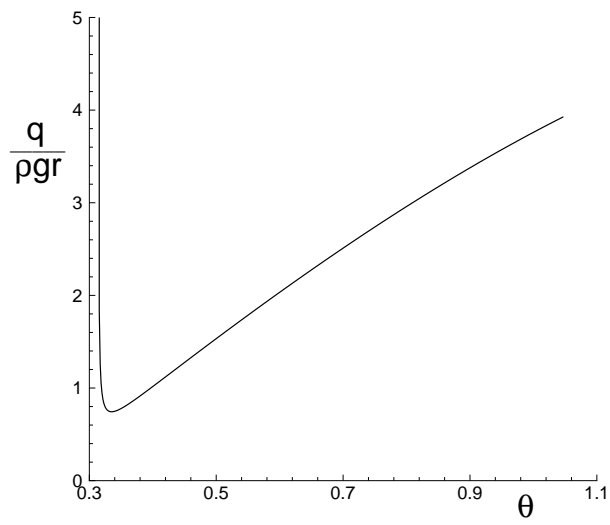


(d).

Figure 5.

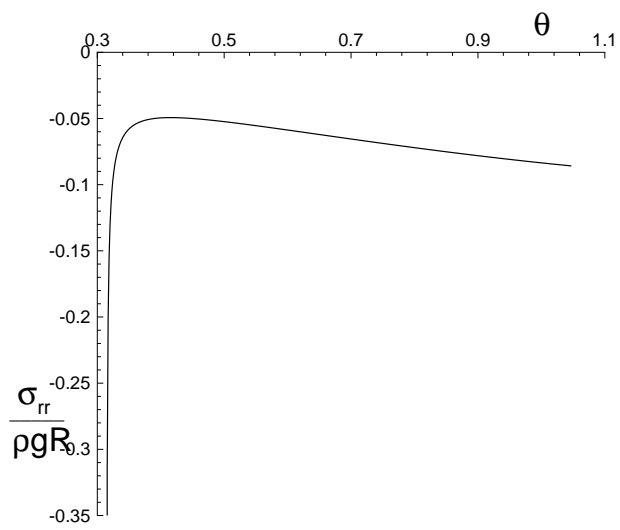


(a).

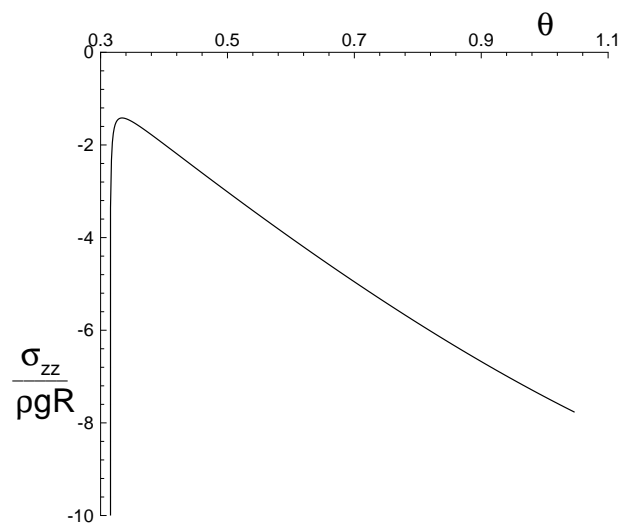


(b).

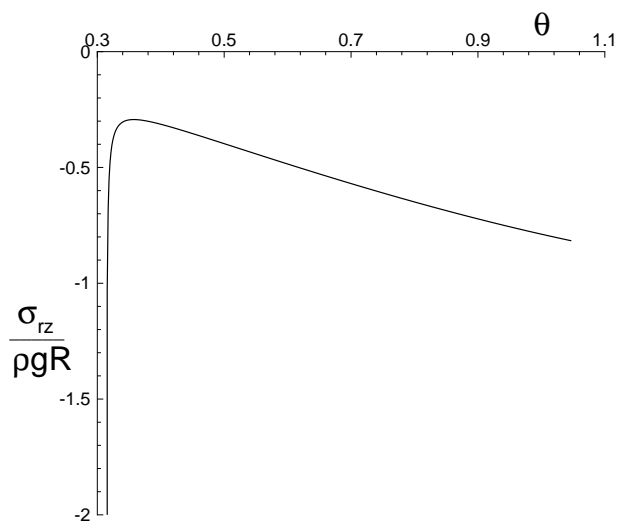
Figure 6.



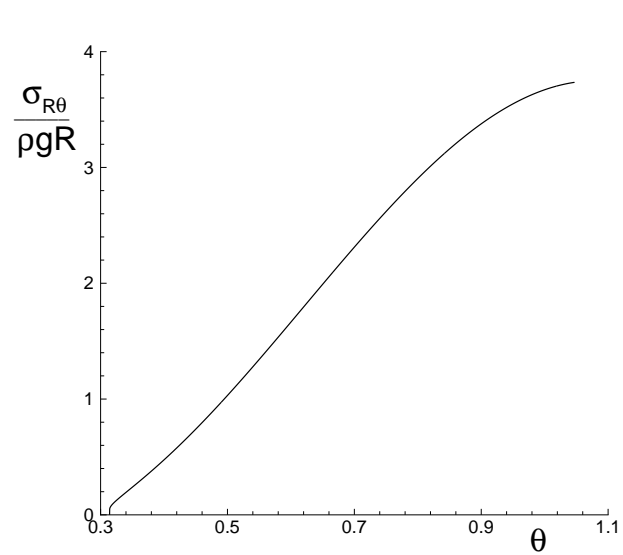
(a).



(b).

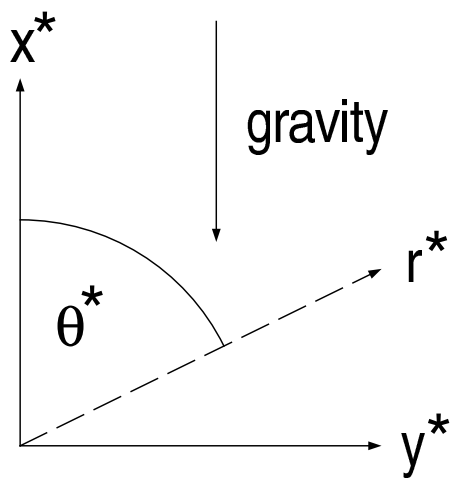


(c).

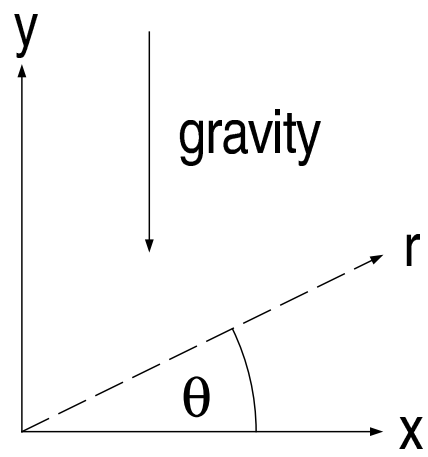


(d).

Figure 7.



(a).



(b).

Figure 8.